

Supplement of Atmos. Chem. Phys., 20, 2031–2056, 2020  
<https://doi.org/10.5194/acp-20-2031-2020-supplement>  
© Author(s) 2020. This work is distributed under  
the Creative Commons Attribution 4.0 License.



*Supplement of*

## **Merging regional and global aerosol optical depth records from major available satellite products**

**Larisa Sogacheva et al.**

*Correspondence to:* Larisa Sogacheva (larisa.sogacheva@fmi.fi)

The copyright of individual parts of the supplement might differ from the CC BY 4.0 License.

# Supplementary material

## S1 Regions of interest

For details, see Sect. 2.1

**Table S1. Geographical coordinates (latitude, longitude) and coverage (land, ocean) for the studied regions (as in Fig.1).**

	area (short name)	coverage	latitude	longitude
1	Europe (Eur)	land	36°N - 60°N	15°E - 50°E
2	Boreal (Bor)	land	60°N - 85°N	180°E - 180°E
3	Asia, North (AsN)	land	40°N - 60°N	50°E - 165°E
4	Asia, East (AsE)	land	5°N - 41°N	100°E - 130°E
5	Asia, West (AsW)	land	5°N - 41°N	50°E - 100°E
6	China, South-East (ChinaSE, subregion)	land	20°N - 41°N	103°E - 135°E
7	Australia (Aus)	land	10°S - 45°S	100°E - 155°E
8	Africa, North (AfN)	land	12°N - 36°N	17°W - 50°E
9	Africa, South (AfS)	land	35°S - 12°N	17°W - 50°E
10	South America (SA)	land	55°S - 5°N	35°W - 82°W
11	North America, West (NAW)	land	13°N - 60°N	100°W - 135°W
12	North America, East (NAE)	land	13°N - 60°N	55°W - 100°W
13	Indonesia (Ind)	land/ocean	10°S - 5°N	90°E - 165°E
14	Atlantic Ocean, dust (AOd)	ocean	5°N - 30°N	17°W - 47°W
15	Atlantic Ocean, biomass burning (AOB)	ocean	30°S - 5°N	17°W - 9°E

## S2 AOD spatial distribution

Mapped annual offsets were calculated from the median AOD for all products available at 550 nm (Fig. S1, upper panel). Year 2008 was chosen as the focus of this exercise, as AOD data are available from most instruments (Sect. 2.2). Additional composites were calculated for 2000 and 2017 as TOMS, VIIRS, and EPIC were not available for 2008 (note TOMS is also unavailable for 2017 and VIIRS/EPIC for 2000). Median AOD is slightly higher in 2008 over both land (0.185) and ocean (0.133), and thus globally (0.147), compared with 2000 and 2017 over land (0.169/0.174), ocean (0.124/0.132) and globally (0.137/0.145), respectively. However, all these differences remain below 0.011. Although AOD is higher over ChinaSE in 2008 compared to other years, similar AOD spatial patterns are observed for the 3 years chosen for the inter-comparison. Thus, using those 3 years (2000, 2008, 2017) to compare global, annual-averaged AOD deviation from the median AOD, is suitable for revealing systematic large-scale differences among the products.

Over land, TOMS AOD is about twice as high (by 0.173) as the median land AOD for all available products (0.169); OMI is higher by 0.066. One possible explanation is potential cloud contamination, related to the lower sensor resolution compared to the other instruments. Global AOD is also higher for POLDER by 0.036, over both land (by 0.040) and ocean (by 0.033), except for the dust area AfN, where AOD is lower than the median.

Products from different instruments retrieved with similar algorithms (AVHRR DB/SOAR, SeaWiFS, VIIRS), often show similar patterns. AVHRR DB/SOAR and SeaWiFS tend to underestimate AOD compared to the median, whereas VIIRS global AOD provides only a small overestimation (by 0.006) of the median value. MODIS DT&DB show higher AOD compared to the median; the deviation of Terra DT&DB from the median (by 0.032 for both land and ocean) is about twice as high as that for Aqua DT&DB (by 0.018 and 0.015 for land and ocean, respectively). This offset between the two MODIS sensors has been reported previously; although time-of-day differences might contribute, it is thought to be dominated by calibration offsets, and has improved compared to previous data versions (Levy et al., 2018; Sayer et al., 2019).

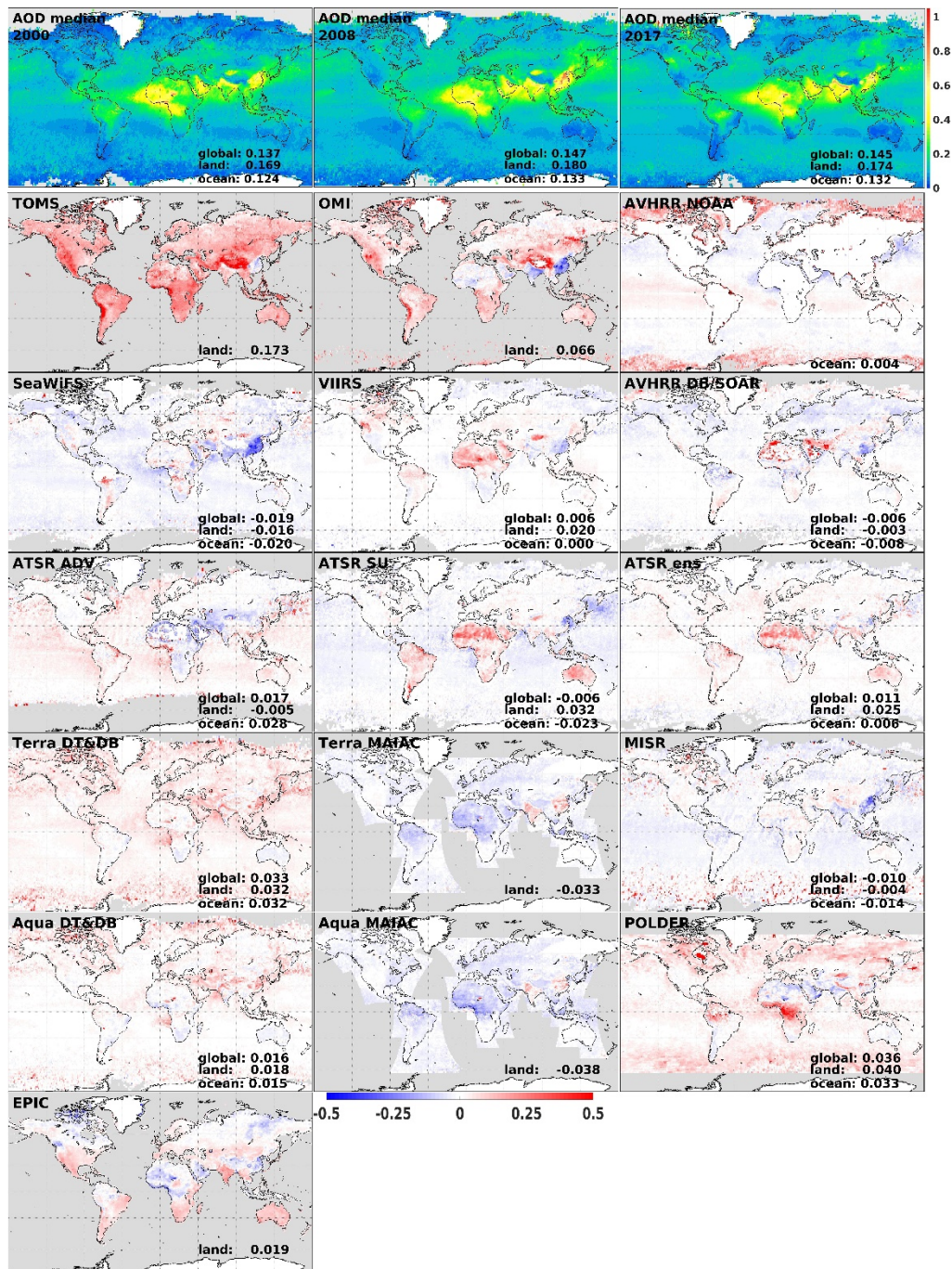


Figure S1. Upper line: annual AOD median for 2000 (left), 2008 (middle) and 2017 (right), calculated from the products available at 550nm. Lines 2-6: AOD deviation (anomalies) of the different products from the annual median AOD for years 2000 (TOMS), 2017 (VIIRS and EPIC) or 2008 (all other products). Global land and ocean AOD mean differences are shown for each product, when available. For JJA, see Fig. S1.

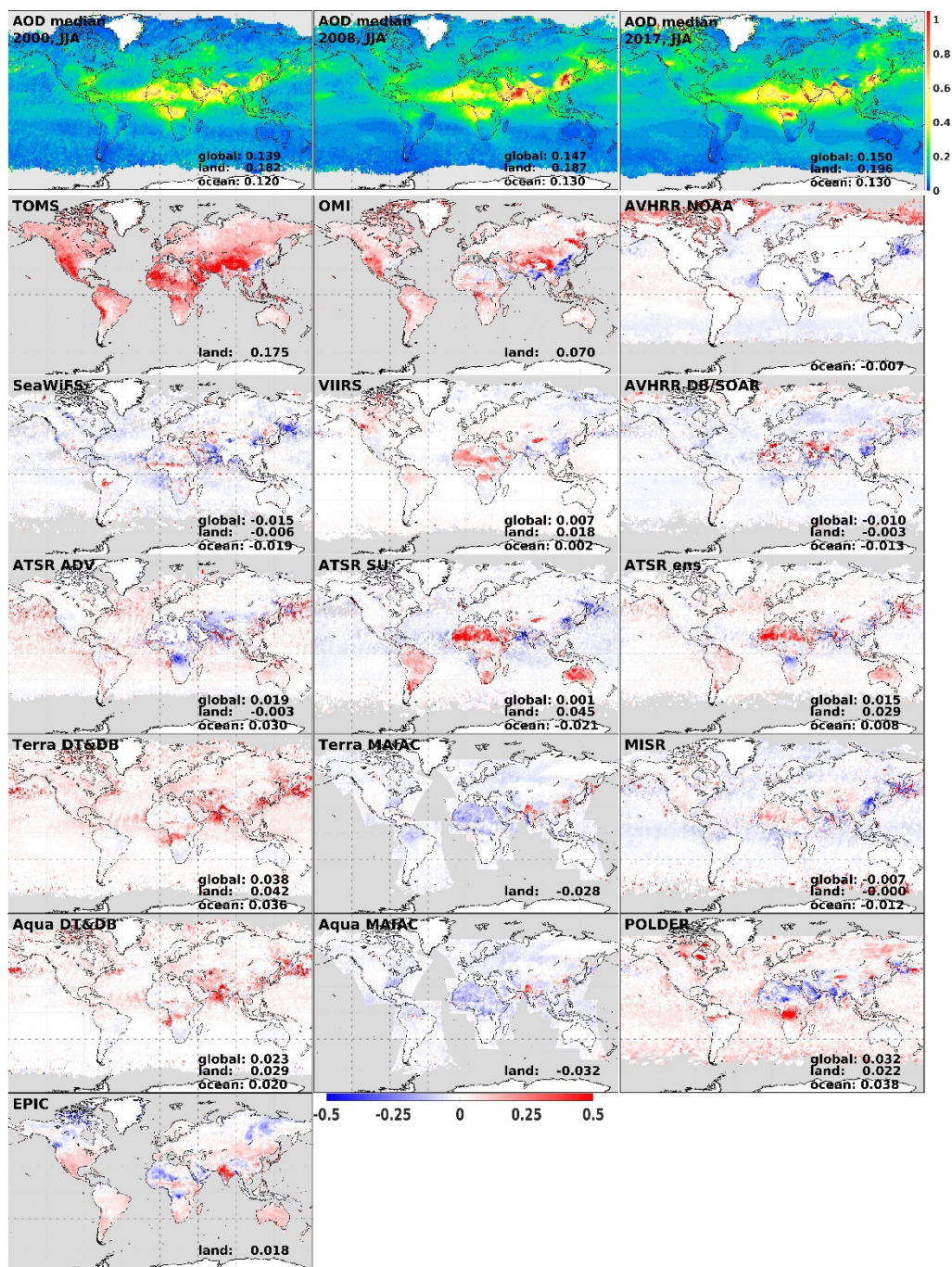


Figure S2. Upper line: JJA AOD median for 2000 (\*), 2008 and 2017 (X), calculated from the available products. Lines 2-6: AOD deviation of the different products from the annual median AOD for years 2000 (TOMS), 2017 (VIIRS and EPIC) or 2008 (all other products). AOD anomalies with respect to the AOD median are shown on the deviation plots. Global land and ocean AOD mean differences are shown for each product, when available.

Interestingly, different algorithms applied to the same or similar instruments often show opposite results, providing an algorithmic spread from the median value. Unlike MODIS DT&DB, both MODIS MAIAC AOD values are lower than the median over land (by 0.033 and 0.038 for Terra and Aqua, respectively). ATSR ADV is slightly higher over ocean (by 0.029), whereas ATSR SU is lower than the ocean median by a similar amount (0.023). Over land, ATSR ADV is lower, especially over bright surfaces (Sect. 2.6.1), if retrieved, whereas ATSR

SU is considerably higher over bright surfaces, compared to the median value. As a result, ATSR ADV AOD underestimates (by 0.005) and ATSR SU overestimates (by 0.032) the median AOD over land.

Together these results imply that algorithmic approach (i.e. pixel selection and retrieval assumptions) can have at least as strong an influence as sensor calibration/sampling differences on the differences between monthly L3 products, at least when assessed on an annual basis.

The global land and ocean AOD values are within  $\pm 0.03$  of the median AOD for most products, which is within the Global Climate Observing System (GCOS) goal requirement of the greater of 0.03 or 10% (GCOS, 2016). However, contrasting behaviour appears in several regions. In ChinaSE, OMI, AVHRR DT/SOAR, SeaWiFS, VIIRS and MISR AOD are considerably lower (up to -0.25) than the median AOD, whereas the MODIS-family (Terra DT&DB, Aqua DT&DB, Terra MAIAC, Aqua MAIAC) retrieve up to 0.2 higher AOD than the median. Over bright surfaces (e.g., AfN, AsW), VIIRS, ATSR SU, ATSR ensemble retrieves up to 0.2-0.25 higher AOD than the median, whereas the MAIAC-family (Terra MAIAC, Aqua MAIAC, EPIC) AOD is lower by up to 0.1-0.15 than the median. Over the open oceans, the VIIRS and ATSR ensemble show AOD closest to median among the products.

As there is no clear deviation from the median for almost all products over open ocean in the continental outflow areas (e.g. AOd and AO<sub>b</sub>), this confirms that the datasets contain similar AOD in these regions. The phenomenon of high Southern Ocean AOD is found in several satellite data sets, including MODIS Terra and Aqua DT, MISR and POLDER and may be related to either emissions of marine aerosol due to strong winds in the storm track zones (e.g., Hoskins and Hodges, 2005), or unresolved clouds (e.g., Toth et al., 2013; Witek et al., 2018).

Seasonal deviations from the median AOD are similar to the annual patterns throughout the year. However, the spread among the products is slightly more pronounced in JJA (June, July, August; Fig. S3, Northern Hemisphere summer), when the absolute AOD often reaches its maximum in certain regions (e.g., in China, Sogacheva et al., 2018a).

As both negative and positive deviations are observed in regions with high AOD, surface type and optical models are likely to influence the AOD retrieval. High AOD might, in turn, be wrongly screened as cloud and thus bias monthly AOD lower. As with many factors that contribute significantly to AOD retrieval results, surface treatment and cloud screening should be tested with L2 (higher-resolution, swath-based) daily data; this is beyond the scope of the current study, which examines only L3 monthly AOD products.

### S3 Diversity of the satellite AOD

To further reveal differences among the AOD products retrieved with different algorithms and applied to different satellites, the diversity of the satellite annual mean AOD ( $AOD_{div}$ ) was calculated, as in Chin et al., (2014):

$$AOD_{div} = 0.5 \frac{AOD_{max} - AOD_{min}}{AOD_{median}} * 100\%$$

The seasonal AOD diversity (Fig. S3) was calculated for 2000, 2008 and 2017 from all 16 products. As expected, satellite data agree best over ocean, and diversity decreases from 2000 (40-60%) towards 2017 (20-30%). Higher over-water diversity is often seen in high latitude oceans, for which retrievals are more challenging due to cloud cover and the steep solar zenith angle, which leads to both more limited sampling and more retrieval artefacts (Toth et al., 2013). Note that our results differ from Chin et al. (2014) as we include additional satellite products (and in some cases newer versions of the products than available during the 2014 study). The diversity is considerably higher over land, reaching more than 90% over certain areas in year 2000 (NAW, SA, Siberia, central Asia, AfS and Aus). AOD diversity decreases considerably in 2017 (to 30-40% on average), when AOD from only NASA Earth Observation System (EOS) (MISR, MODIS) and related NOAA (VIIRS) satellites is currently available, and the extent of high-diversity areas is lower. Australia stands out as the region where AOD averages disagree most, showing >90% AOD diversity irrespective of the year or number of satellites/products available. This is in great part due to the fairly persistent low AOD in the region, such that small offsets between data sets result in a large relative diversity. The diversity is somewhat higher in summer, which is also clear from the comparison between annual (Fig. S1) and summer (Fig. S2) AOD deviation from the median value. AOD diversity for products used for merging (see Sect.4-6 for details) are shown in Fig. S4.

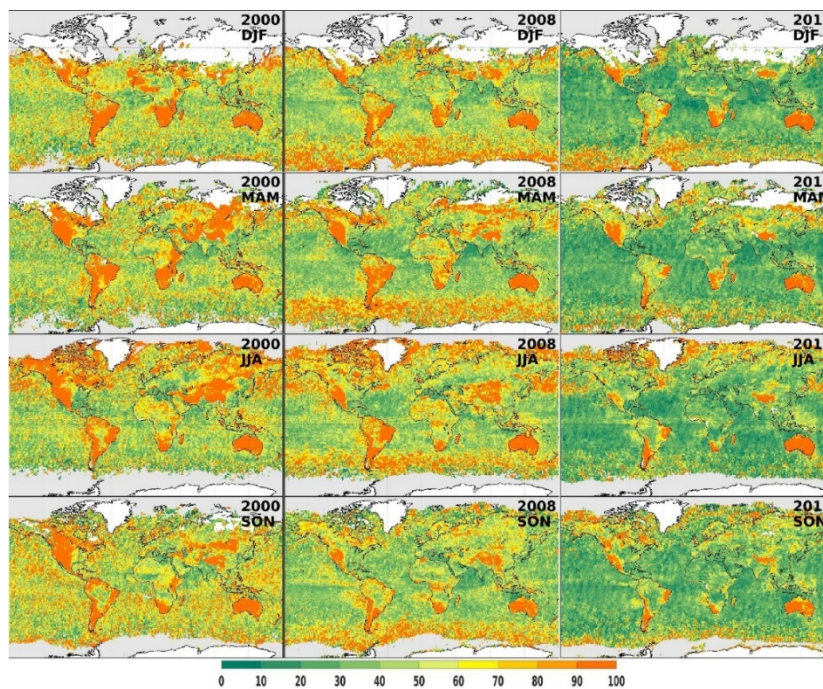


Figure S3. Seasonal mean AOD diversity for years 2000, 2008 and 2017 for all 16 available products.

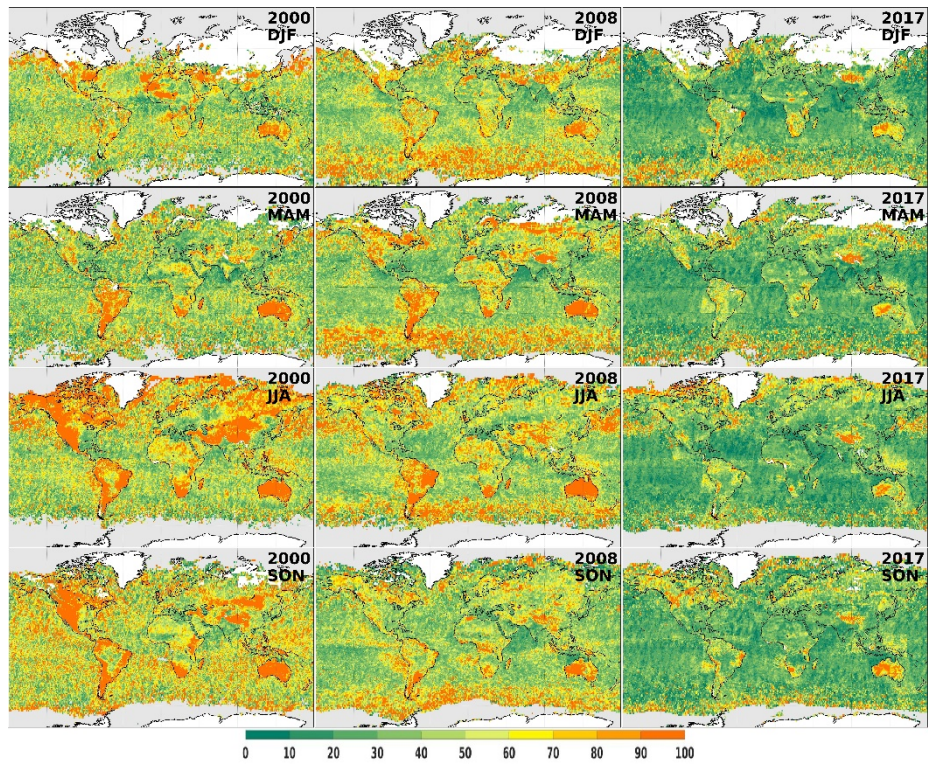


Figure S4. Seasonal mean AOD diversity for years 2000, 2008 and 2017 for all products used for merging (Table 2).

## S4 Aerosol type classification with AERONET

For details, see Sect. 3.1

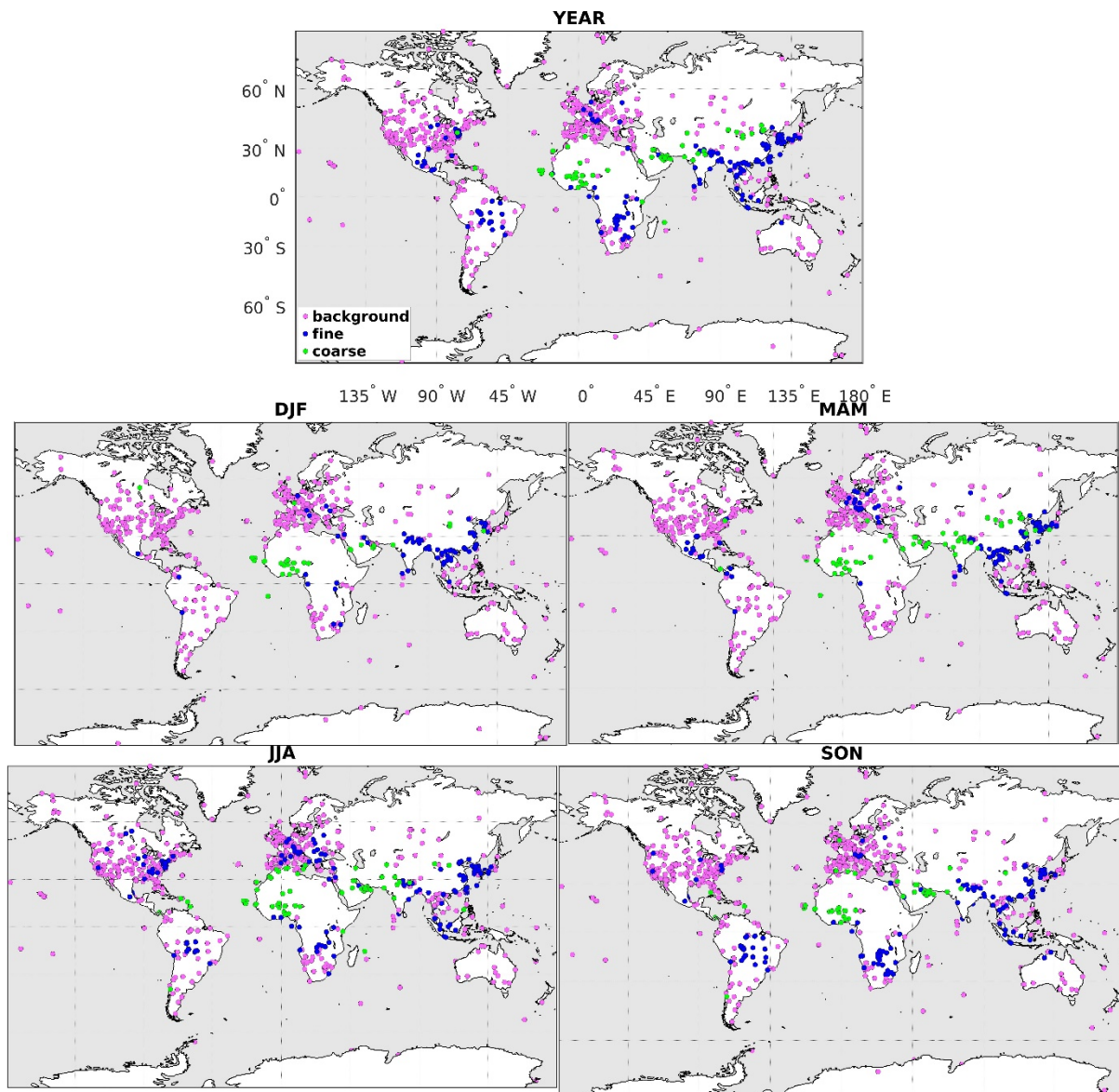


Figure S5. Mean annual and seasonal classification of the AERONET stations for the period of 1995-2017 based on AOD and AE. For background aerosol type (purple), AOD  $\leq 0.2$ ; fine-dominated aerosol type (blue) is at AOD  $> 0.2$  and AE  $> 1$ ; coarse-dominated aerosol type (green) is at AOD  $> 0.2$  and AE  $< 1$ .



## S5 Binned offset, global evaluation

For details, see Sect. 3.1.1

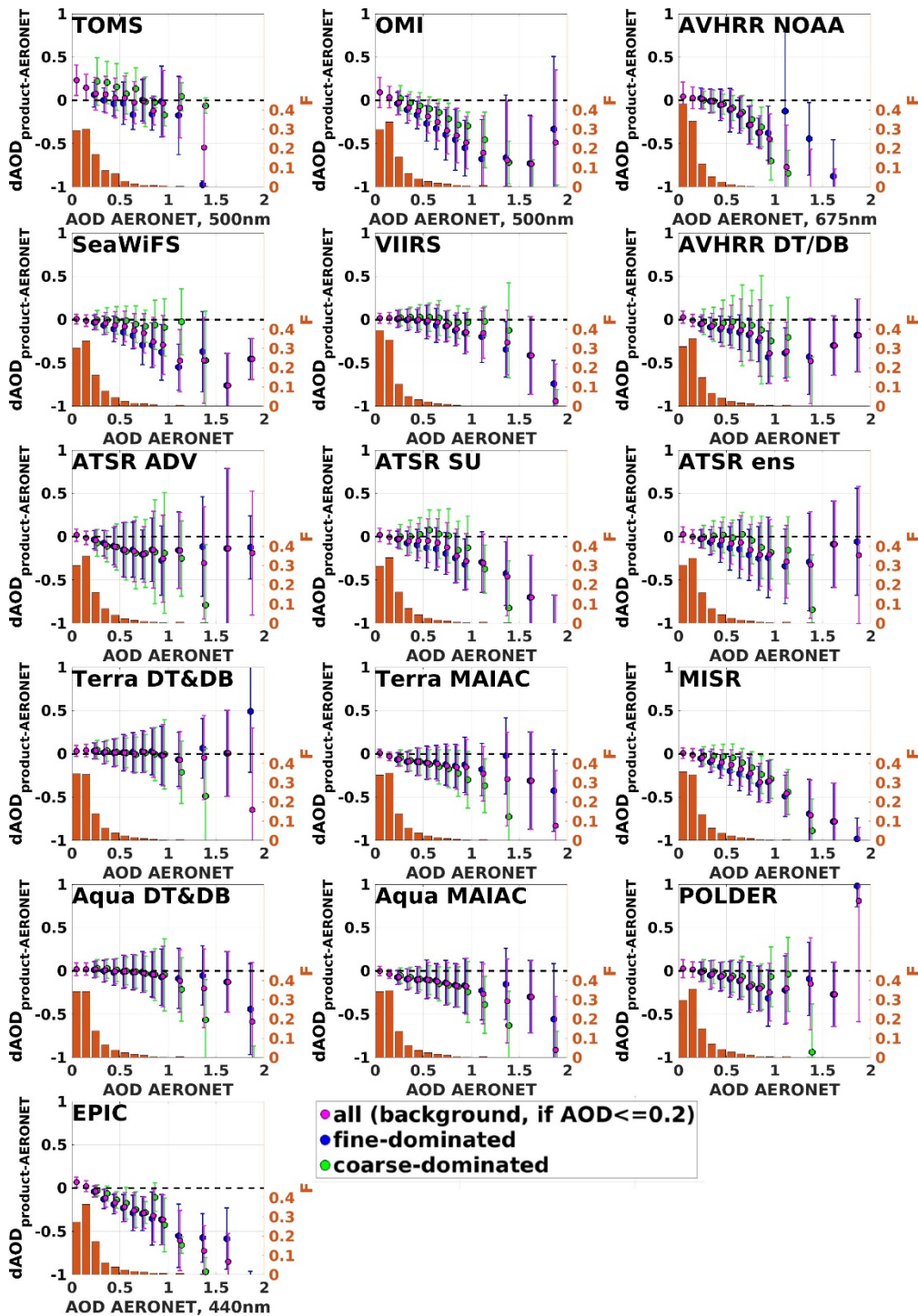
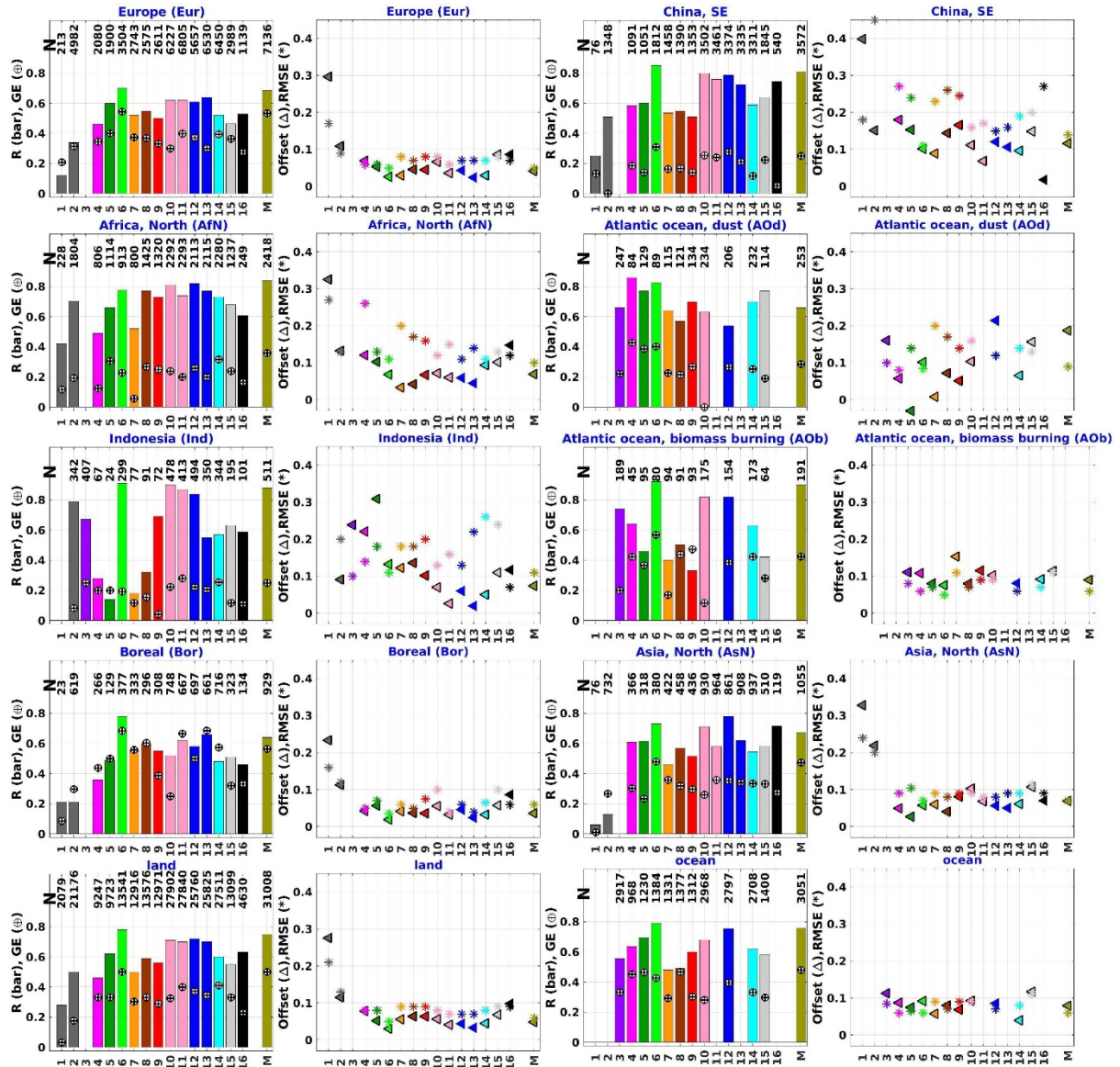


Figure S6. Difference between satellite and AERONET monthly AOD for selected AOD bins: median bias (circles), bias standard deviation (error bars) for all AOD types (purple), background aerosol (purple, AOD ≤ 0.2), fine-dominated AOD (blue) and coarse-dominated AOD (green); fraction of points in each bin (bar, orange).

## S6 AOD evaluation over selected regions

For details, see Sect. 3.1.2



- |           |                 |            |                |                  |
|-----------|-----------------|------------|----------------|------------------|
| 1 TOMS    | 3 AVHRR_NOAA    | 7 ATSR_ADV | 10 Terra DT&DB | 14 MISR          |
| 2 OMI     | 4 AVHRR_DT/SOAR | 8 ATSR_SU  | 11 Terra MAIAC | 15 POLDER        |
| 5 SeaWiFS | 6 VIIRS         | 9 ATSR_ens | 12 Aqua DT&DB  | 16 EPIC          |
|           |                 |            | 13 Aqua MAIAC  | M Merged product |

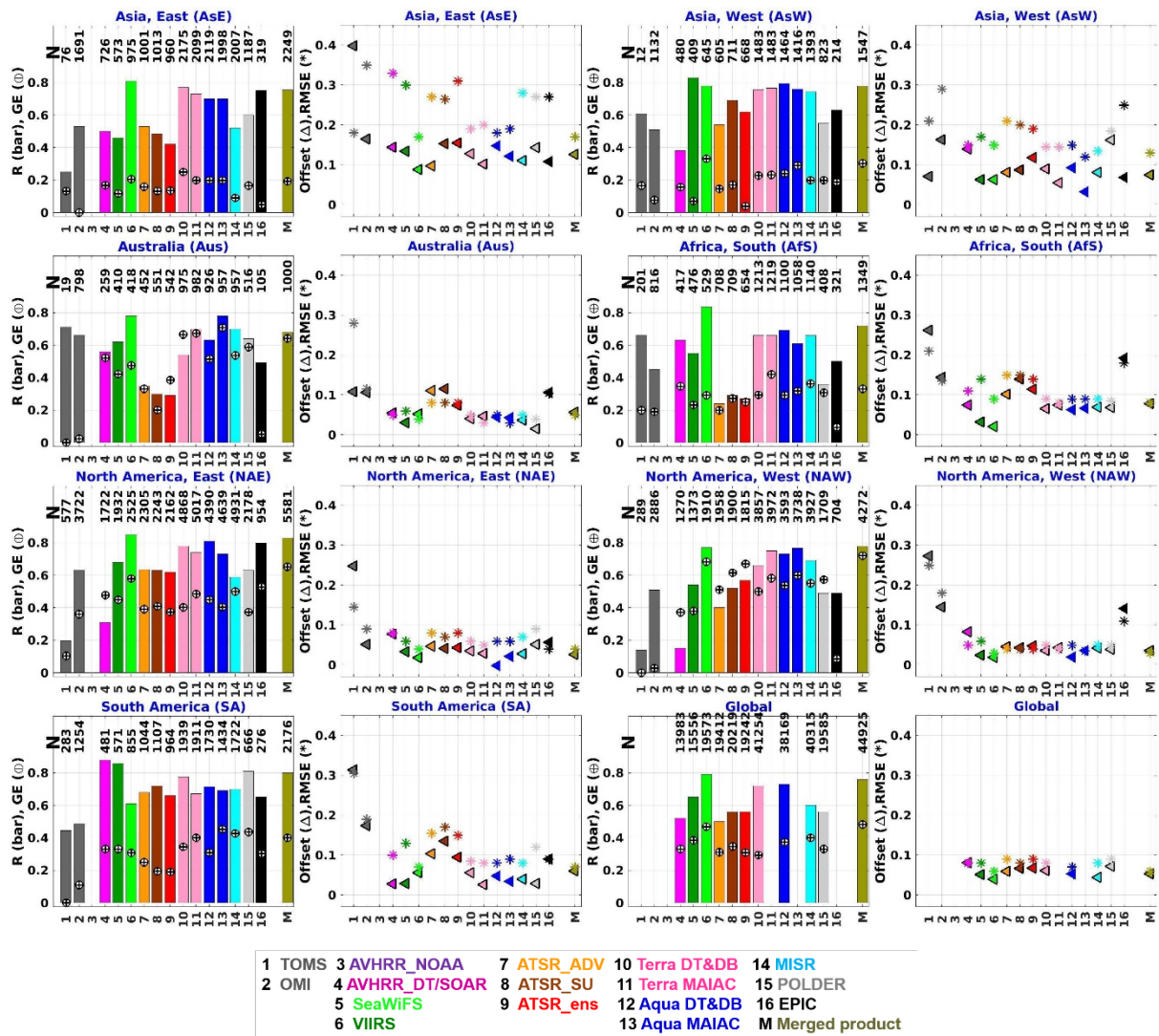
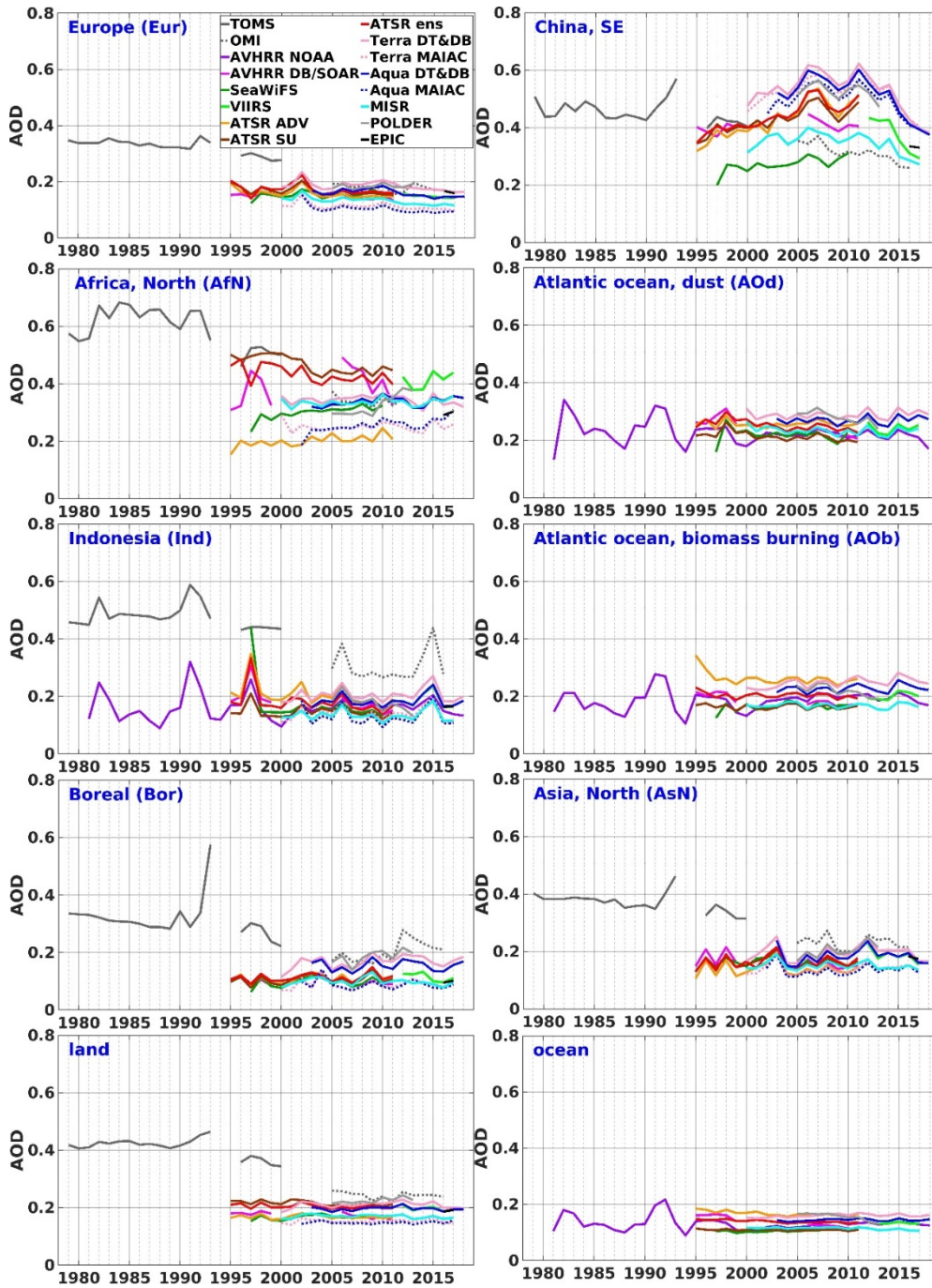


Figure S7. AERONET evaluation statistics for all studied regions: correlation coefficient  $R$ , bar; fraction of pixels satisfying the GCOS requirements,  $GE$ ,  $\oplus$ ; Offset (satellite product-AERONET),  $\Delta$ ; root mean square error RMSE,  $*$  for AOD monthly aggregates for each product (1:16, legend for products below the plot) and the L3 merged product (M, approach2, RM2 for all aerosol types, for details see Sect.4.2) with corresponding colours (legend) for all selected regions (as in Fig. 1). N is a number of matches with AERONET. Note, for products which do not provide the global coverage (e.g., no retrieval over oceans), the results are missing.

## S7 AOD time series

For details, see Sect. 3.2.



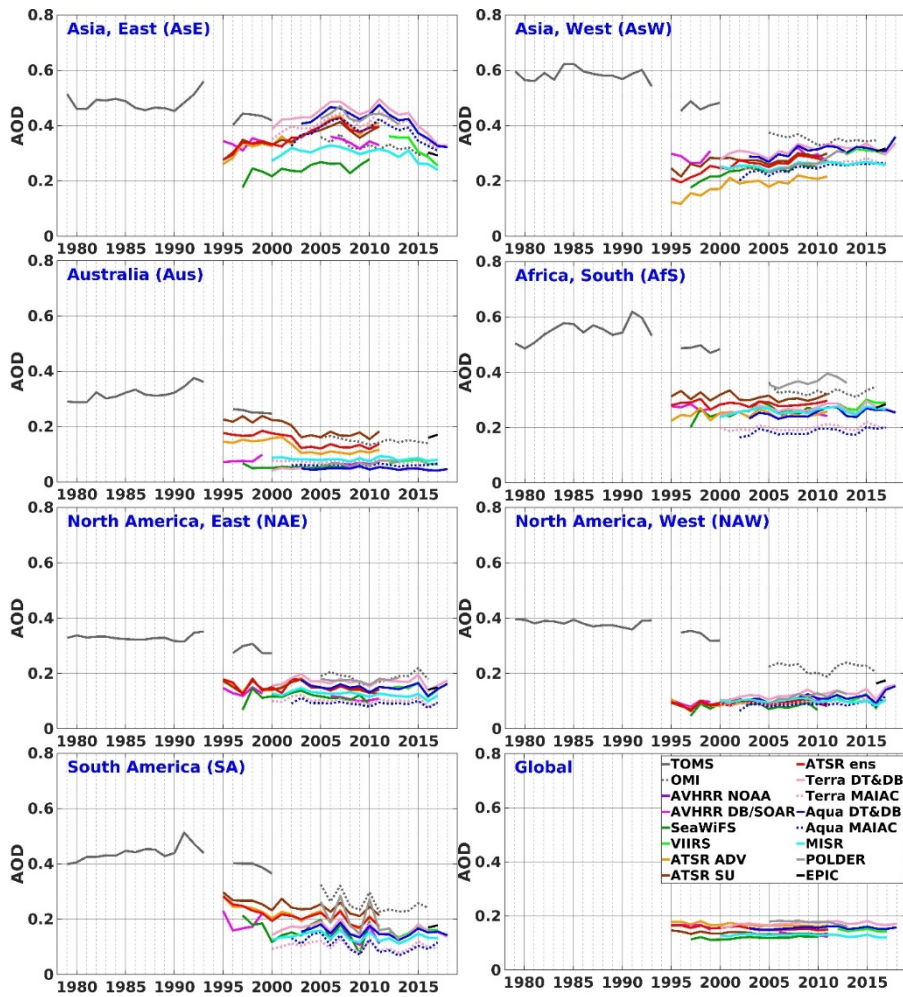
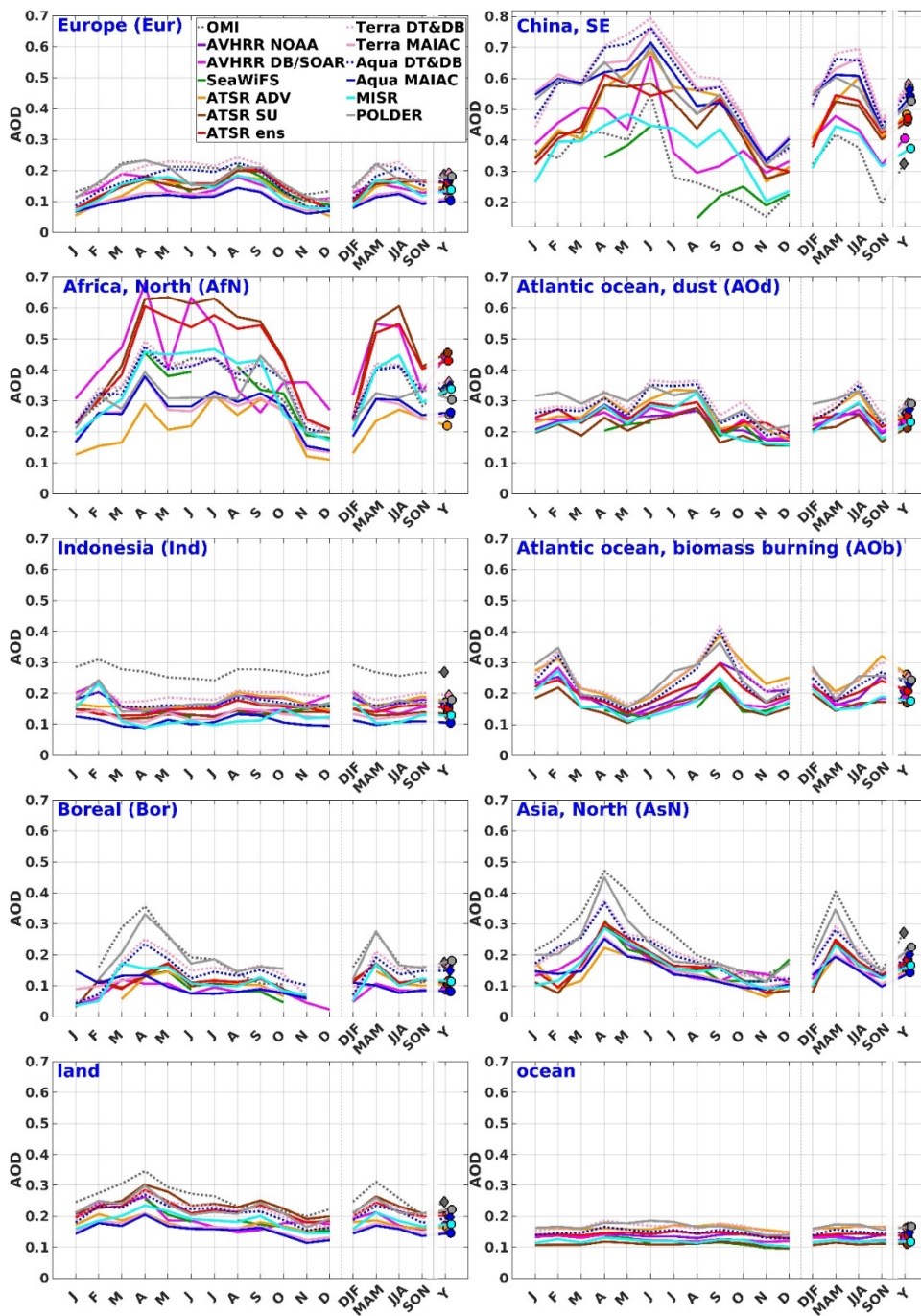


Figure S8. Annual AOD time series from different products (see legend) for all selected regions.

## S8 AOD annual cycles

The year 2008 was chosen for annual AOD cycle comparisons for the aforementioned reasons. Annual cycles (Fig. 7 and Fig. S7) agree better in regions with relatively low AOD (e.g., in Europe). In Europe, the relative increase towards MAM and second peak in August-September is captured by all products. In ChinaSE, where AOD loading and annual variation are higher, the AOD increase towards June and another AOD peak in September are observed. Outbreaks of biomass burning aerosols over the Atlantic produce clear peaks in February and September, as shown in all available products. Thus, besides the similar interannual variation among the satellite products, the AOD annual cycles among the products are also similar.



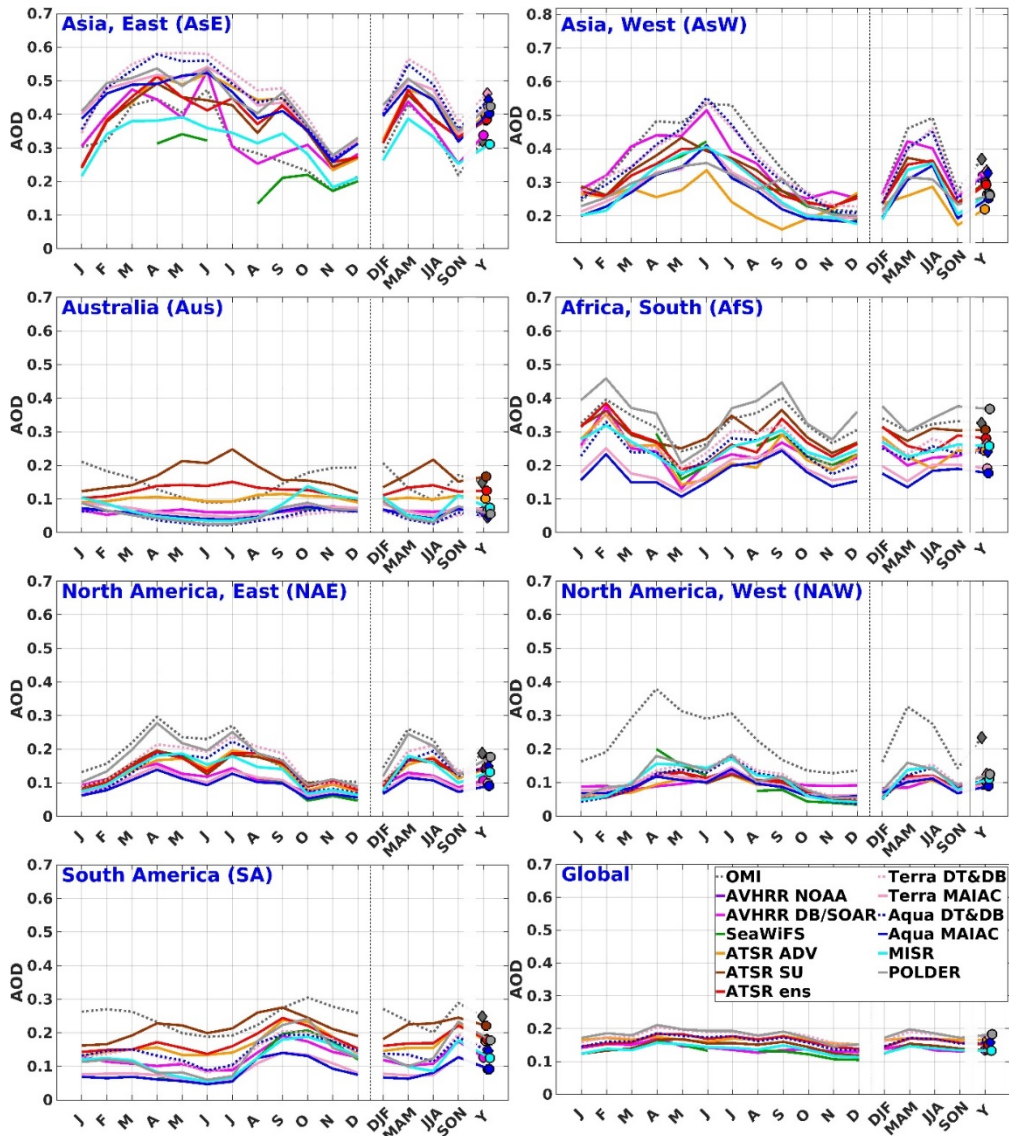


Figure S9. Monthly (J for January, F for February, etc.) and seasonal (DJF, MAM, JJA, SON) AOD time series and yearly aggregated AOD for 2008 (Y) for available products (see legend) for all selected regions.

## S9 Regional offsets

For details, see Sect. 4.1.2.

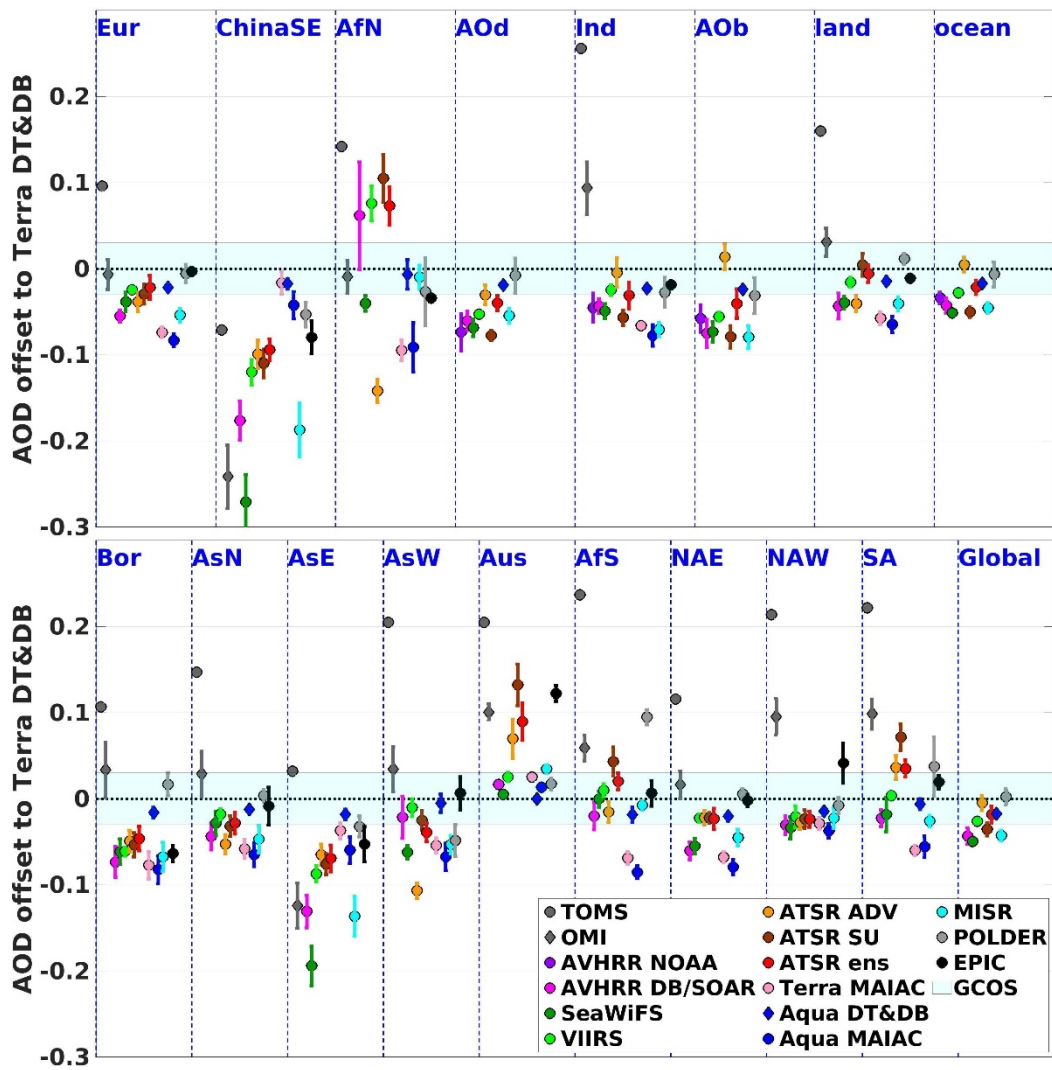
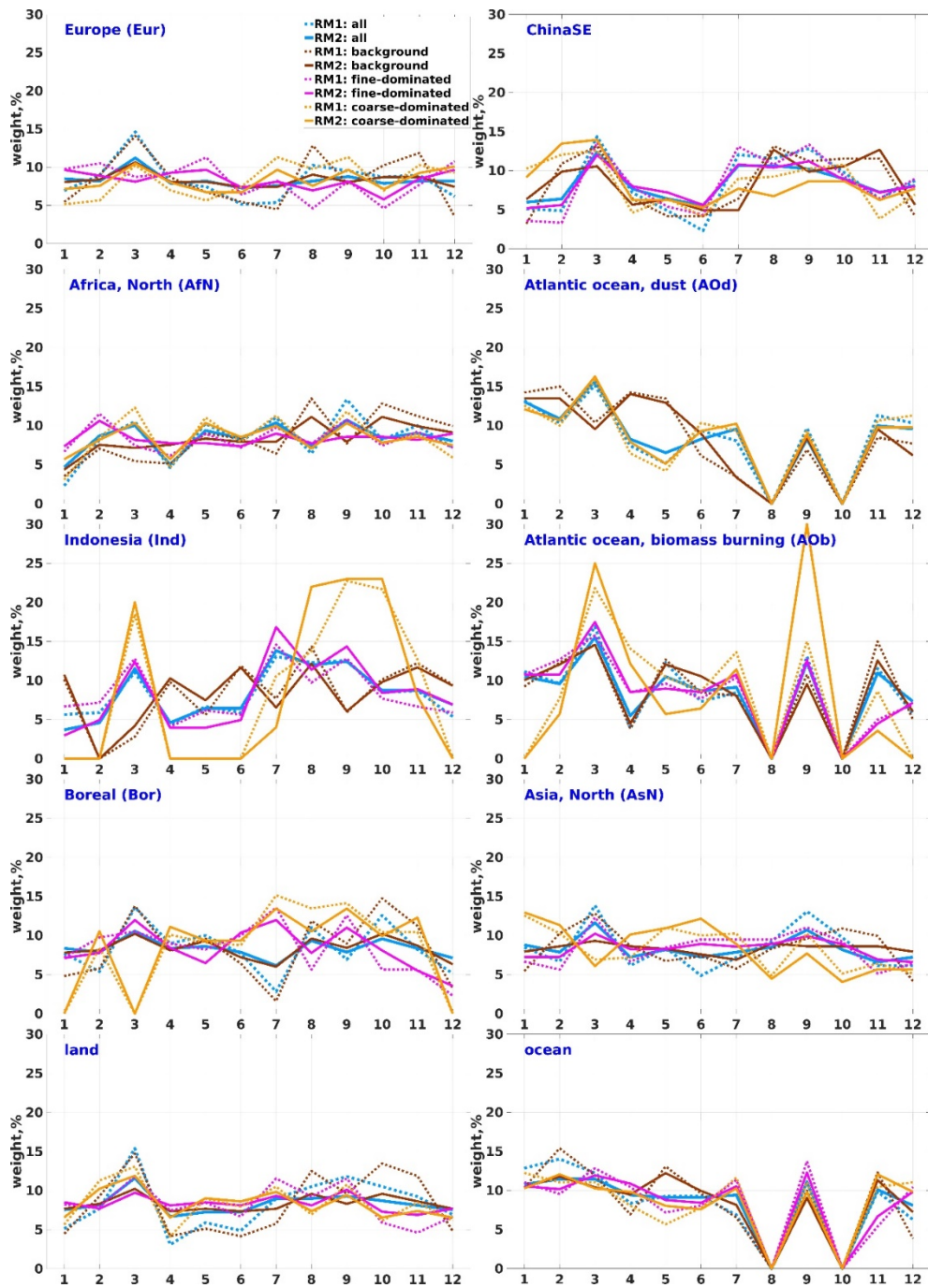
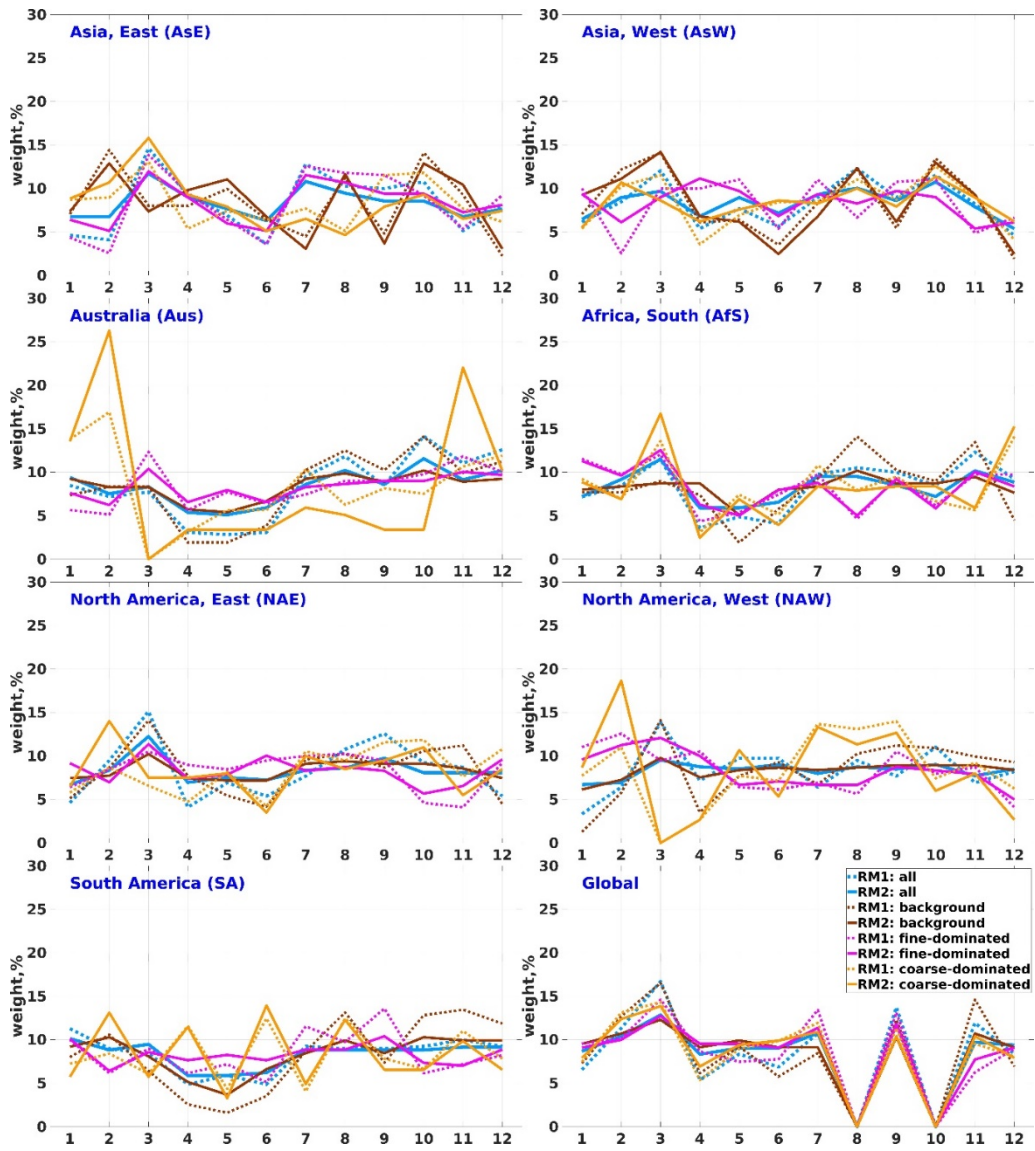


Figure S10. Regional annual average AOD offset between each dataset and the ATSR\_ensemble dataset. GCOS requirement for  $\pm 0.03$  AOD is shown as a background color.

## S10 Weights of each individual product

For details, see Sect. 4.2.2.





- |                 |            |               |               |
|-----------------|------------|---------------|---------------|
| 1 AVHRR DB/SOAR | 4 ATSR_ADV | 7 Terra DT&DB | 10 Aqua MAIAC |
| 2 SeaWiFS       | 5 ATSR_SU  | 8 Terra MAIAC | 11 MISR       |
| 3 VIIRS         | 6 ATSR_ens | 9 Aqua DT&DB  | 12 POLDER     |

Figure S11. Weight of each product for the selected regions for different aerosol types.

## S11 Evaluation of the merged AOD products with AERONET

For details, see Sect. 5.1.

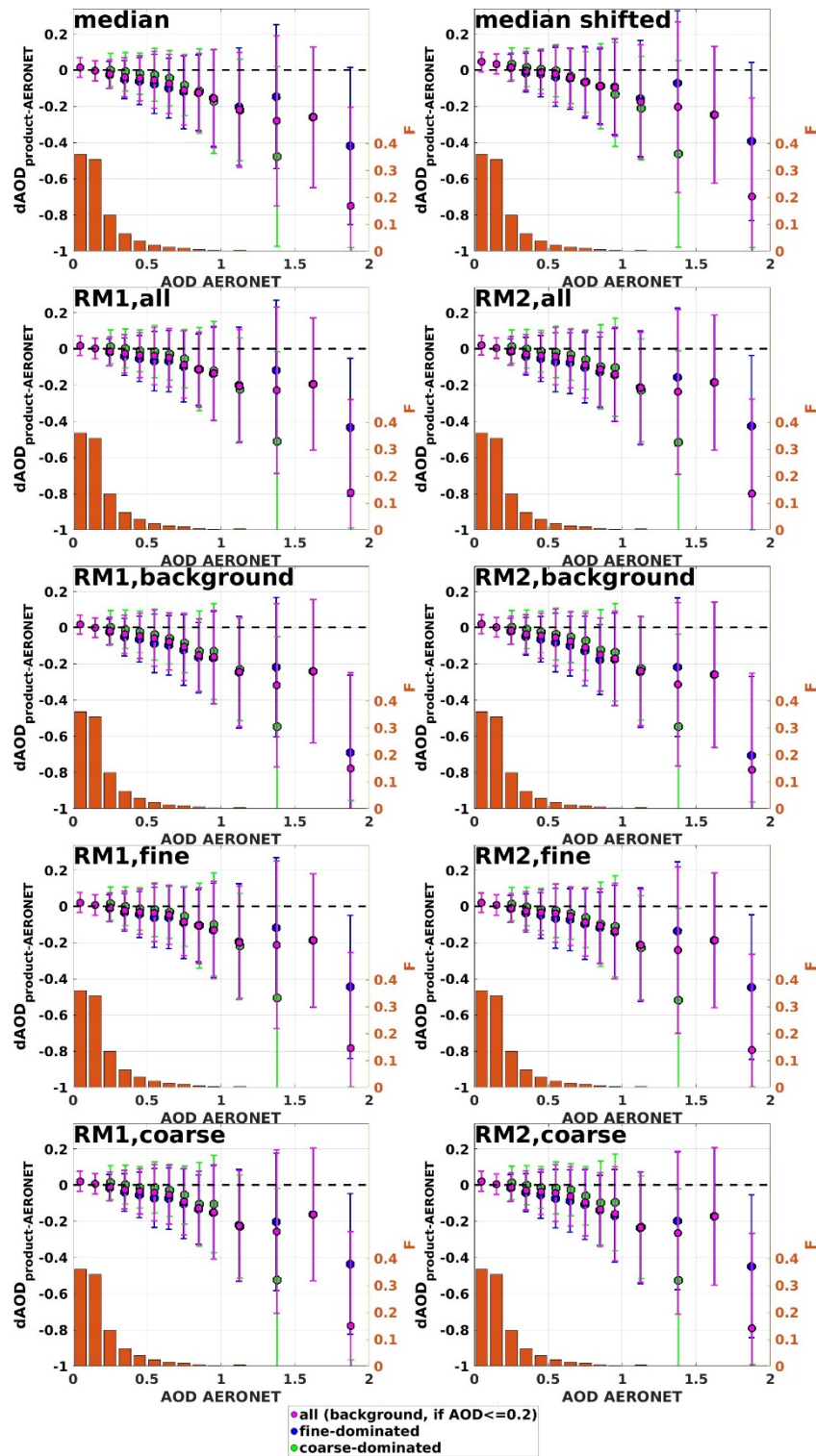
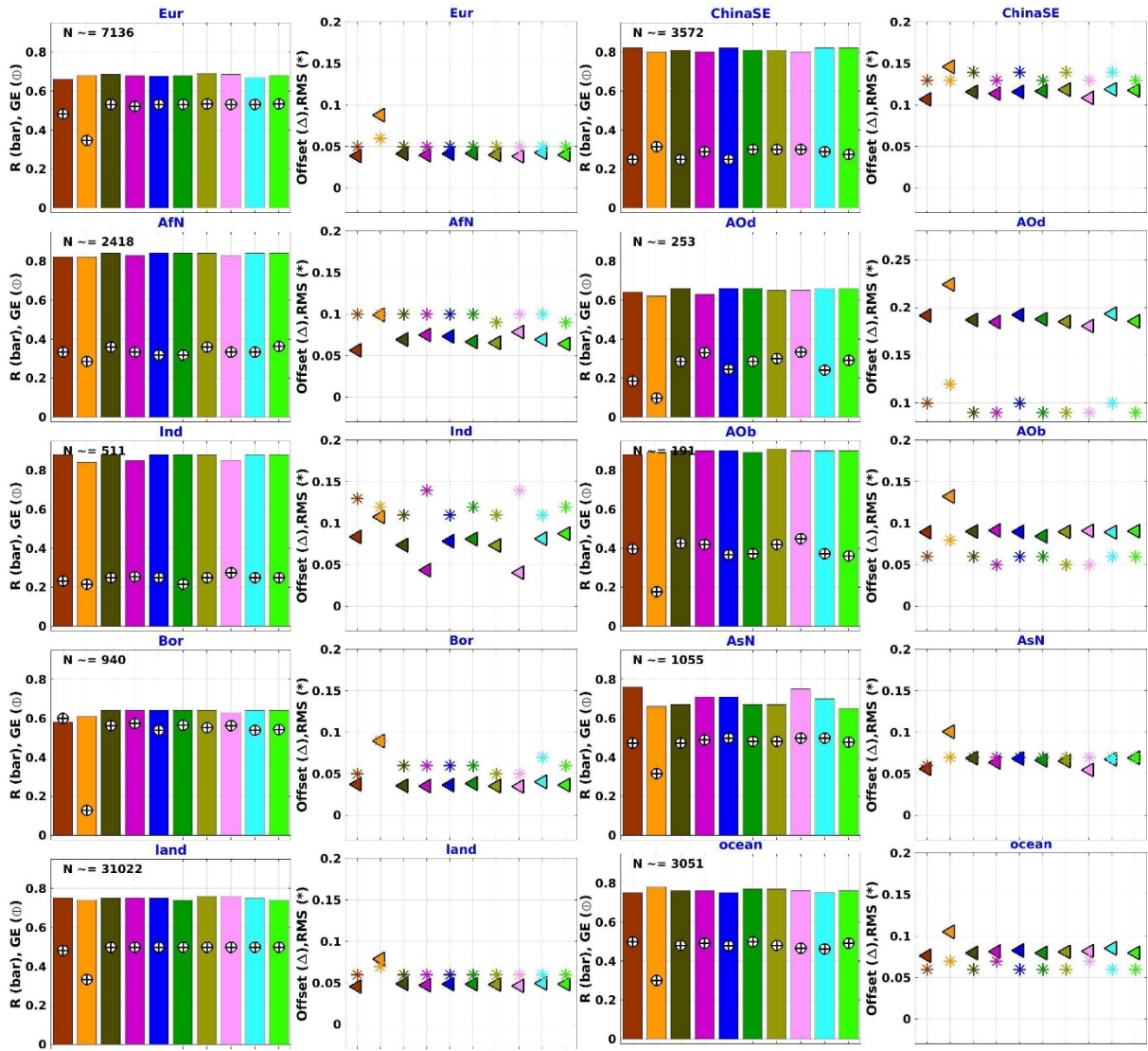


Figure S12. Difference between AOD merged products and AERONET monthly AOD for selected AOD bins: median bias (circles), bias standard deviation (error bars) for all AOD types (purple), background aerosol (purple, AOD $\leq$ 0.2), fine-dominated AOD (blue) and coarse-dominated AOD (green); fraction of points in each bin (bar, orange).



Median      RM1,all   RM1,background   RM1,fine   RM1,coarse  
 Median shifted   RM2,all   RM2,background   RM2,fine   RM2,coarse

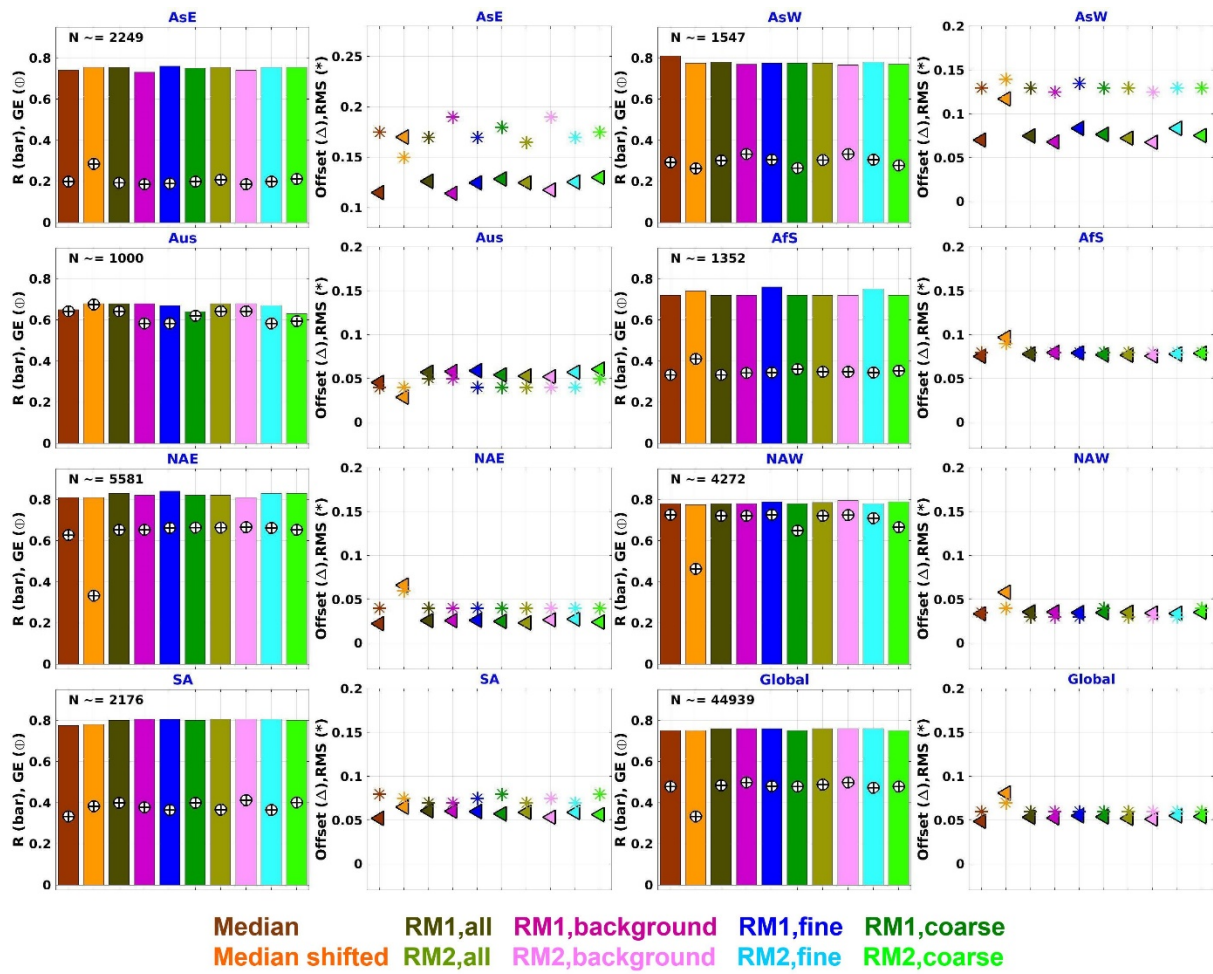


Figure S13. AERONET evaluation statistics: correlation coefficient  $R$ , bar; fraction of pixels satisfying the GCOS requirements,  $GE$ ,  $\oplus$ ; Offset (satellite product-AERONET),  $\Delta$ ; root mean square error  $RMS$ ,  $*$ ) for AOD products merged with different approaches, median, shifted median, RM1, RM2 for different aerosol types for all selected regions.

**S12 Annual and seasonal AOD regional offsets between individual products and the merged product**

For details, see Sect. 5.2.3.

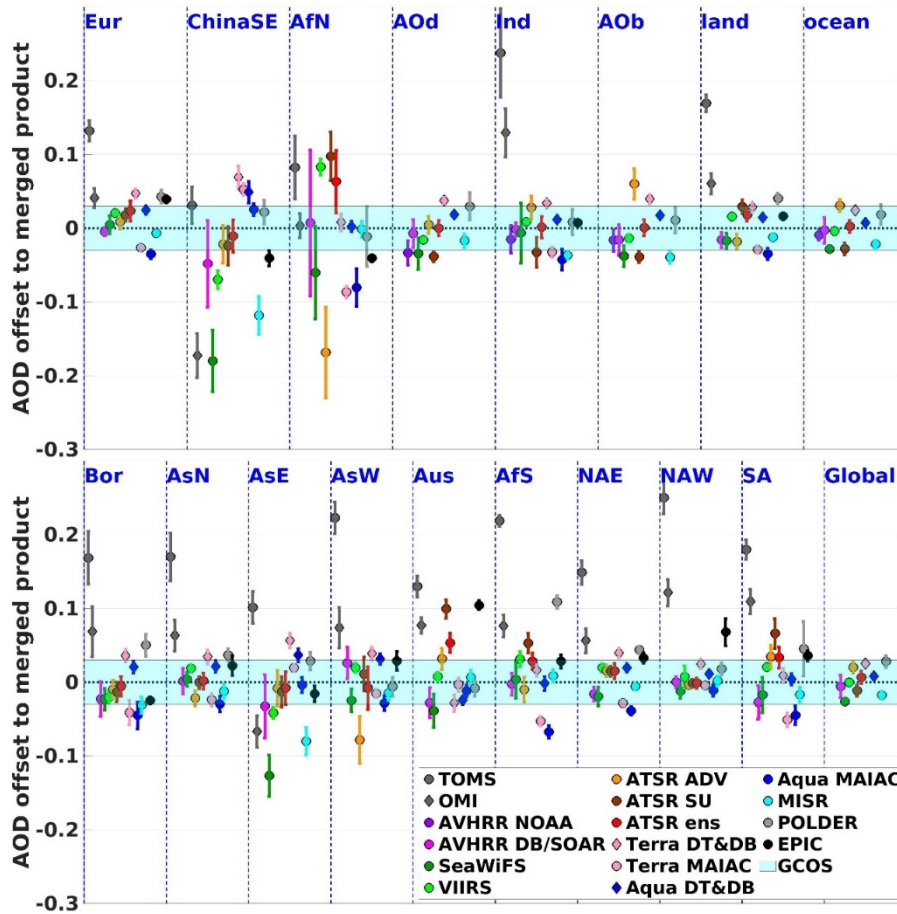


Figure S14. Regional annual AOD offset between individual products and the merged product

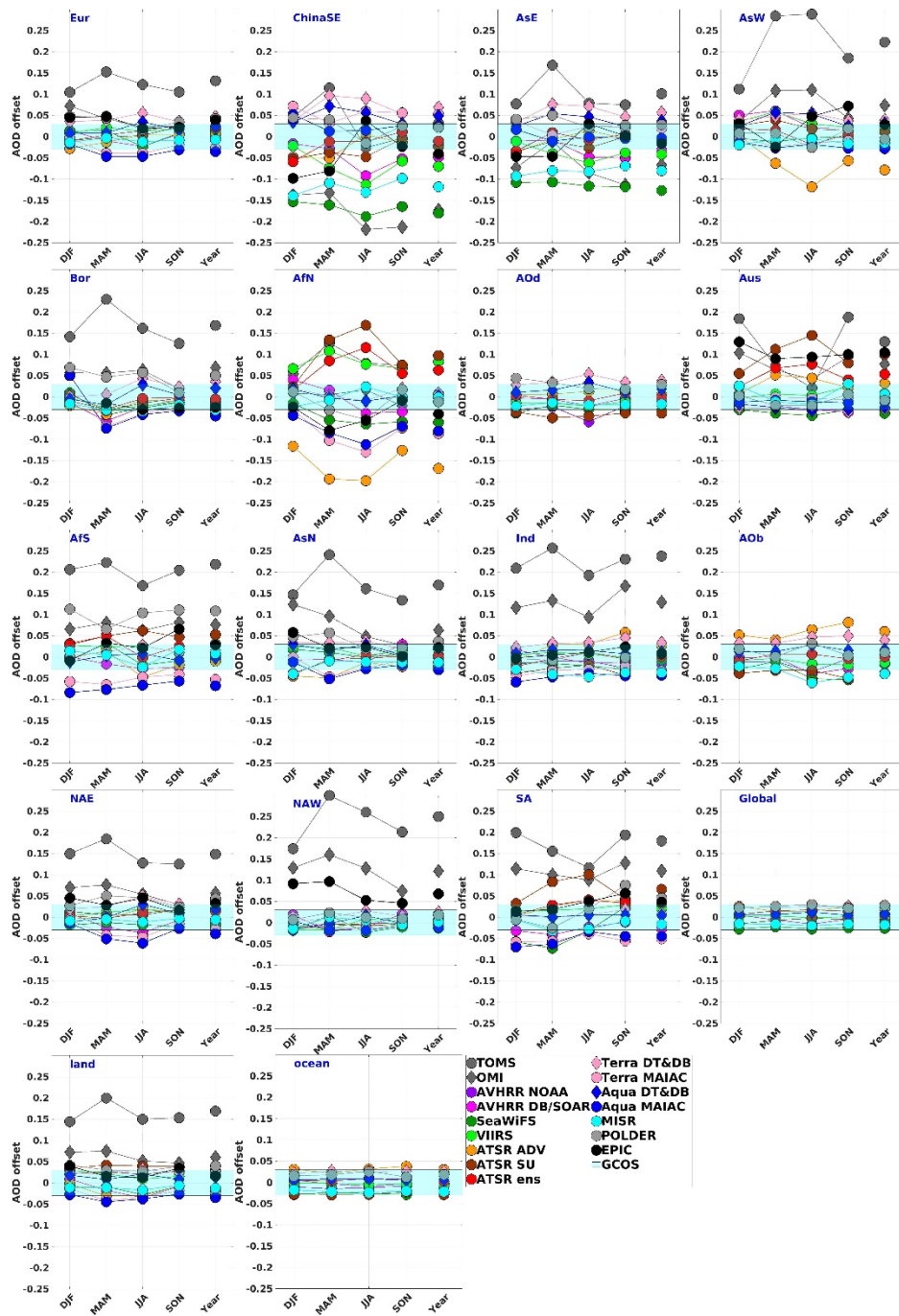
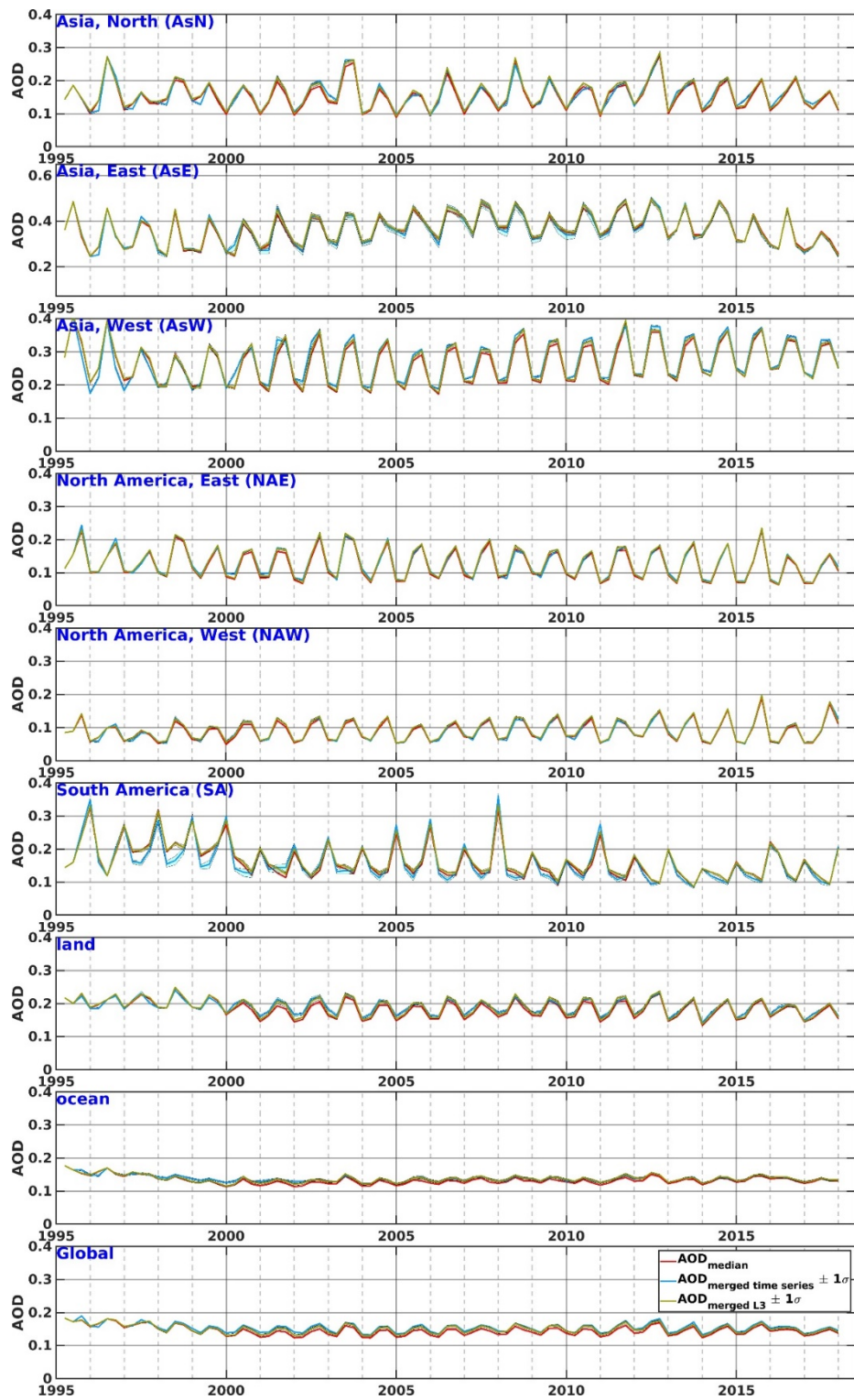


Figure S15. Seasonal (DJF, MAM, JJA, SON) and annual (Year) offsets between AOD from individual products (legend) and merged AOD product, for all selected regions.

### S13 Seasonal and monthly merged AOD time series

For details, see Sect. 6.



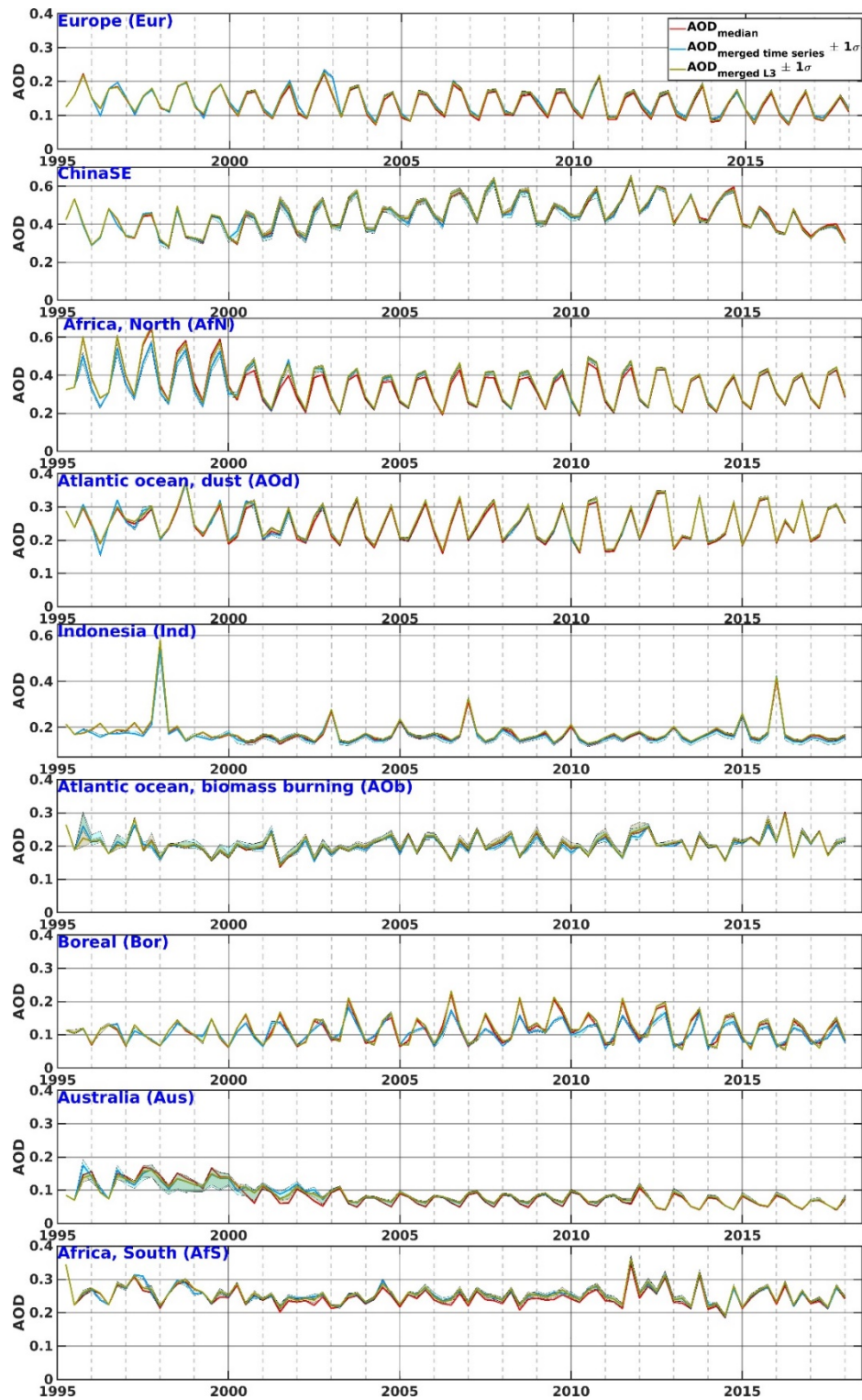
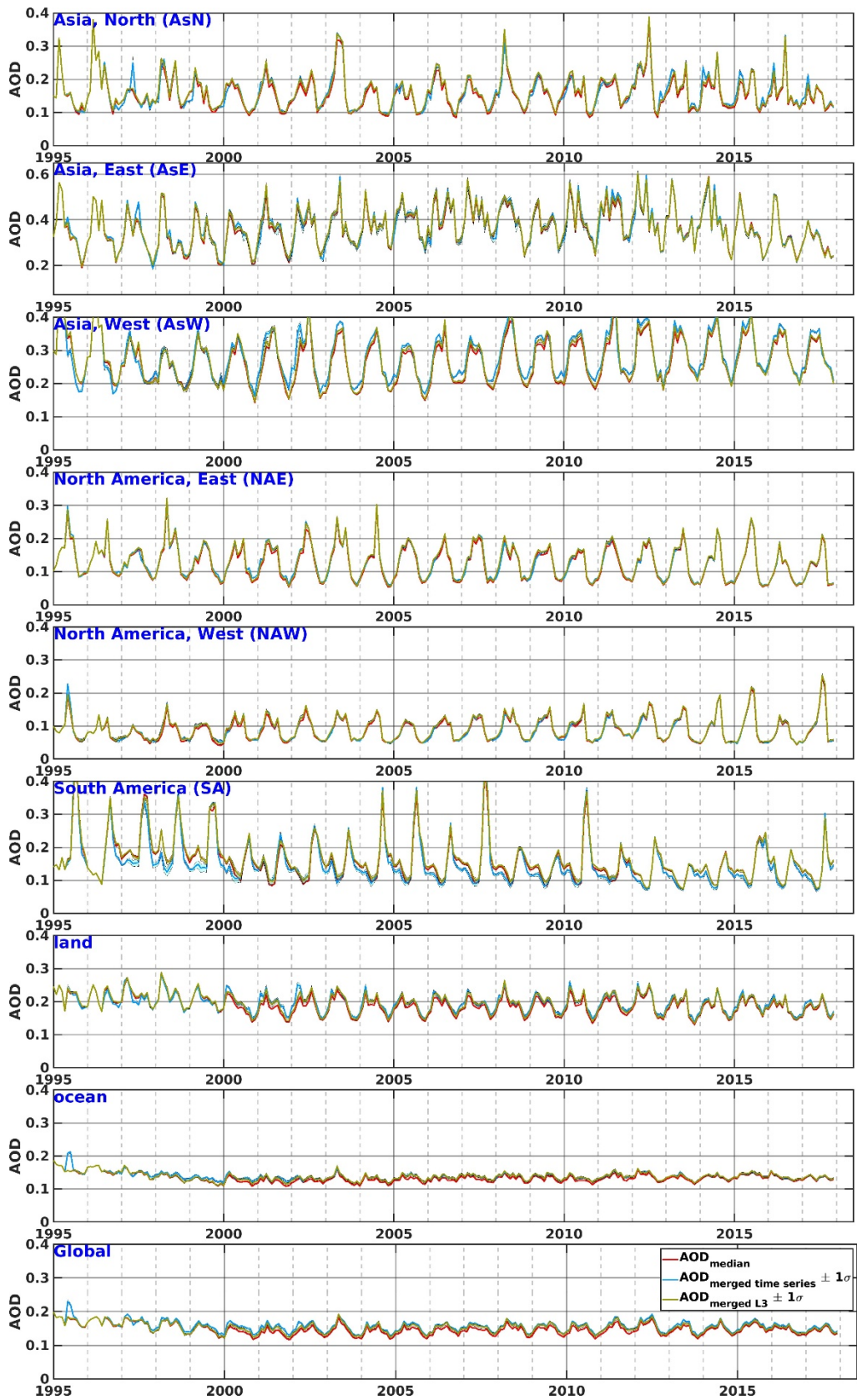


Figure S16. Seasonal AOD median time series (red), merged time series (blue) and time series from the merged L3 product (olive) for all studied regions. AOD  $\pm 1\sigma$  for the merged time series and for the time series from the merged L3 products are shown as light blue and light olive shadows, respectively. Note the different scale.



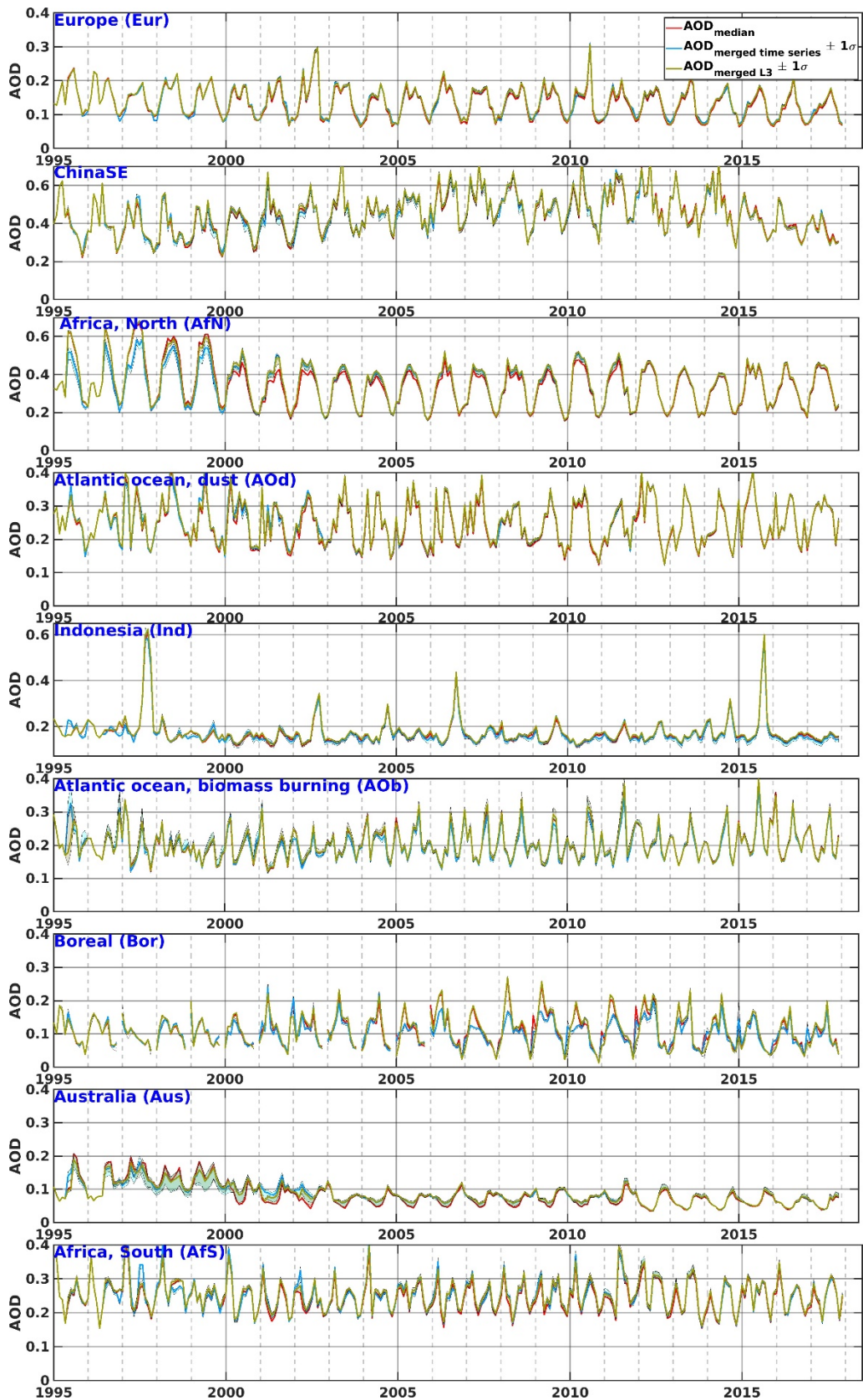


Figure S17. Monthly AOD median time series (red), merged time series (blue) and time series from the merged L3 product (olive) for all studied regions. AOD  $\pm 1\sigma$  for the merged time series and for the time series from the merged L3 products are shown as light blue and light olive shadows, respectively. Note the different scale.

### S14 Discrepancy between the time series from the merged L3 product and merged time series

For details, see Sect. 6.

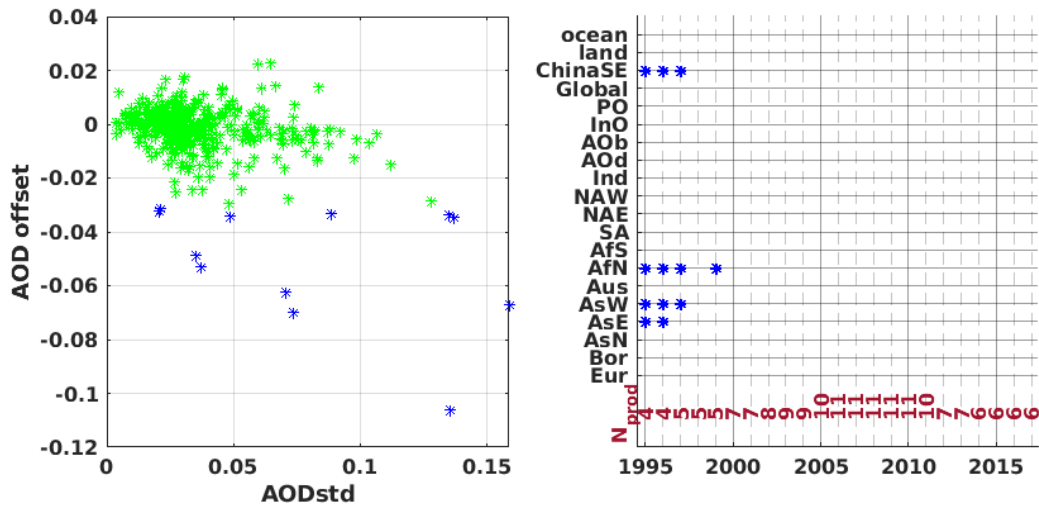


Figure S18. Left: scatterplot for AOD standard deviations (AODstd) between the available products and offset between time series. Green stars– offset within the GCOS requirements of 0.03, red and blue stars – positive and negative (respectively) offset outside the GCOS requirements. Right – annual distribution of the offsets outside the GCOS requirements and number of the products (Nprod) used for merging for each year.

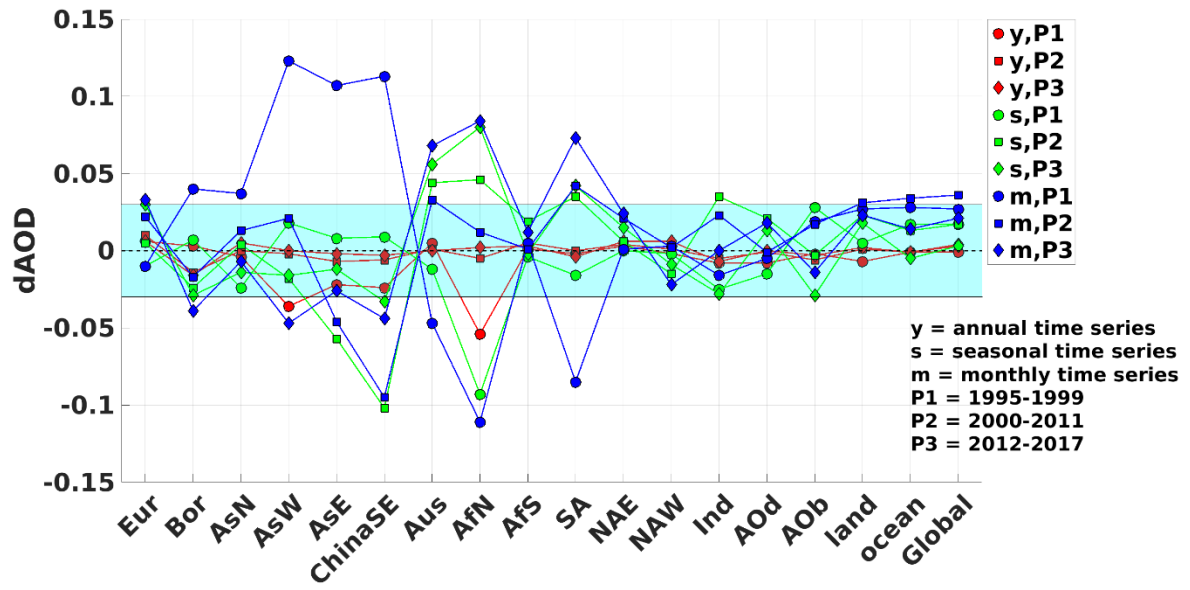


Figure S19. Regional offsets (dAOD) between the annual, seasonal and monthly merged time series and time series calculated from the merged L3 data